available at www.sciencedirect.com

ScienceDirect

journal homepage: www.elsevier.com/locate/agrformet

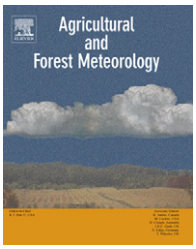

Estimating daytime subcanopy respiration from conditional sampling methods applied to multi-scalar high frequency turbulence time series

C. Thomas [a,*], J.G. Martin [a], M. Goeckede [a], M.B. Siqueira [b,f], T. Foken [c], B.E. Law [a], H.W. Loescher [a,d,e], G. Katul [b]

[a] Department of Forest Science, Oregon State University, Corvallis, OR, USA
[b] Nicholas School of the Environment and Earth Sciences, Duke University, Durham, NC, USA
[c] Department of Micrometeorology, University of Bayreuth, Bayreuth, Germany
[d] National Ecological Observatory Network, Boulder, CO, USA
[e] Institute of Arctic and Alpine Research, University of Colorado, Boulder, CO, USA
[f] Departamento de Engenharia Mecânica, Universidade de Brasília, Brasília, Brazil

ARTICLE INFO

Article history:
Received 7 December 2007
Received in revised form
23 February 2008
Accepted 6 March 2008

Keywords:
Coherent structures
Conditional sampling
Ecosystem carbon cycle
Ecosystem respiration
Eddy accumulation
Similarity theory

ABSTRACT

This study presents a new method to estimate daytime respiration from the subcanopy of forests directly from conventional eddy covariance (EC) measurements. The method primarily considers the respiration signal from root, litter and microbial respiration, which are known to be the main components of ecosystem respiration, R_e, as well as decomposition of coarse and fine woody detritus, and respiration from low understory vegetation (forbs, herbs and grasses). The conceptual framework is based on the premise that upward moving air parcels carry a specific and unambiguous signal in their CO_2 and water vapour composition, which can be separated and distinguished into respiration and photosynthesis. The model employed a combination of conditional sampling methods, quadrant analysis and relaxed eddy accumulation with hyperbolic deadbands to identify respiration events and to quantify their flux contribution. Datasets from five sites, most of which had multiple sampling heights, were selected to test this technique among contrasting ecosystems and canopy structures.

Respiration signals were successfully identified in daytime data of all sites. A hyperbolic deadband of size $H = 0.25$ applied to the plane constructed from perturbations of carbon dioxide c and water vapour q densities effectively separated the signals of respiration from photosynthesis. The time fraction of respiration events was $\leq$10% during daytime. The global correlation coefficient $r_{c,q}$ was found to be a universal predictor of this time fraction and was therefore used as a filter to identify periods of a meaningful and extractable respiration signal. Coherent structures, defined as ramp-shaped flow pattern observed in time series in and above forest canopies, are likely to be the underlying transport mechanism for these respiration events.

Daytime subcanopy R_e estimates derived from the new method agreed with those derived from: (i) the intercept of light-response curves and (ii) soil CO_2 efflux chambers for three of the five sites. Limitations were posed by the dense, multi-layered deciduous canopy and the intense vertical turbulent mixing at one coniferous site. In addition, refixation of respired CO_2 by the understorey (CO_2 recycling) may cause an underestimation

* *Corresponding author*. Fax: +1 541 737 1393.
E-mail address: christoph.thomas@oregonstate.edu (C. Thomas).
0168-1923/$ – see front matter
doi:10.1016/j.agrformet.2008.03.002

of daytime R_e or pose a limitation to the method proposed here. An indicator relating the canopy shear length scale, L_s, to the adjustment length scale, L_d, was proposed to predict the skill of the new method, and found to be useful in four of the five sites. Analysis of vertical coupling in the plant canopy using exchange regimes could explain the failure of the new method for the remaining site.

1. Introduction

Daytime respiration from tall-forested ecosystems remains among the least understood components in the total carbon balance. Tall-forested ecosystems pose unique challenges to respiration measurements because of the diversity in respiring ecosystem components (foliage, live woody tissue, fine roots, litter, soil organic matter, coarse and fine woody detritus), and their variable spatial distribution (Law et al., 2001; Rayment and Jarvis, 2000). In addition, the time it takes photoassimilates synthesized in the leaves to be consumed in the root/rhizosphere can amount to several days (Bowling et al., 2002; Ekblad and Hogberg, 2001; Stoy et al., 2007) and pose additional challenges as different ecosystem components respire at different rates with varying temporal offsets as they propagate through the canopy.

The eddy covariance (EC) technique is now commonly deployed in observational networks of atmospheric surface fluxes of energy and CO_2 around the world (e.g., AmeriFlux, CarboEurope, Asiaflux, Canadian Carbon Program) covering a large range of ecosystems, topography and canopy morphology. However, daytime EC flux estimates only provide net CO_2 fluxes, as CO_2 enriched air from sources and CO_2 depleted air from sinks are subject to intense turbulent mixing under the assumption that above-canopy air and subcanopy space including the ground-surface interface are well coupled. Hence, no explicit information is available on daytime respiration rates from such measurements. Partitioning of net carbon fluxes (F_N) into its components fluxes of photosynthesis/assimilation (F_A) and ecosystem respiration (R_e), i.e., $F_N = F_A - R_e$, for *daytime* conditions is necessary for diagnosing biological responses to environmental drivers such as temperature, moisture and nutrients in the carbon balance.

Three methods are commonly used to compensate for the lack of explicit EC-based R_e measurements in daytime conditions: (a) modeling R_e by extrapolating nighttime EC measurements when $F_A = 0$, i.e., $F_N = R_e$; (b) chamber-based estimates of soil, foliage and woody tissue respiration; or by (c) using stable isotopes (^{13}C in CO_2) to partition F_N into component fluxes. The EC method (a) is widely used when integrating the half-hourly or hourly flux estimates F_N, F_A and R_e into their accumulated budgets of net ecosystem exchange (NEE), gross ecosystem productivity (GEP) and total ecosystem respiration (TER), respectively, as it can readily be applied to long-term records of EC measurements without the need for additional experimental and instrumental efforts. R_e and its components are typically modeled using an exponential functional relationship (Lloyd and Taylor, 1994) between (air or soil) temperature and sometimes, soil water content as independent variable(s), and biomass as a scalar for live tissue (e.g., foliage and woody tissue; Ryan, 1991), and nighttime F_N flux estimates under conditions of sufficient turbulent mixing as dependent variables. Contemporary variations of this method, reviewed elsewhere (Reichstein et al., 2005), present uncertainties and challenges. Extrapolating nighttime data is relatively straight-forward and input variables are routinely measured at most flux sites, but a key assumption is that the temperature sensitivity of F_N developed at night holds true for daytime conditions when both magnitude and amplitude of temperatures are typically higher. Moreover, identifying the ecologically adequate integration time scales of R_e as a function of seasonal behaviour of the ecosystem can be challenging. Inhibition of dark respiration in light (Kok effect), and photorespiration lead to additional uncertainty in the relative contribution of foliar respiration to total ecosystem respiration during the day versus night (Sharp et al., 1984).

The scaled up chamber estimates (method b) are best characterized with continuous chamber measurements of soil respiration in enough locations to be representative of the tower footprint, and require intensive seasonal measurements of foliage and live wood respiration with careful scaling up to the ecosystem scale with measurements of tissue mass (Law et al., 1999). Uncertainties in estimates from this method are introduced through scaling up from the individual plant part (leaf, bole) to the ecosystem level, and through determining the relative contribution of each component to the total ecosystem respiration.

The use of stable carbon isotopes (method c) is based on the discrimination against the heavier ^{13}C in CO_2 by photosynthesis (Farquhar et al., 1989), which leads to elevated ^{13}C ratios in the remaining atmospheric CO_2 pool, assuming little or no fractionation occurs in the respiration processes (Lin and Ehleringer, 1997). Combining isotopic composition of CO_2 and flux measurements enables the partitioning of F_N into F_A and R_e during the day (Bowling et al., 2001; Ogee et al., 2003; Wichura et al., 2004; Yakir and Sternberg, 2000; Yakir and Wang, 1996). The isotopic method has the advantage of estimating the component flux in daytime conditions, but isotopic ratios and the isotopic disequilibrium can be highly variable and vary with geographical location and environmental conditions (Knohl and Buchmann, 2005; Yakir and Sternberg, 2000). Frequent sampling is necessary to resolve this issue and is currently (and in the foreseeable future) cost prohibitive.

Because of the availability of high frequency CO_2 and water vapour time series (>10 Hz) from EC systems, a new method is proposed here that can provide estimates of the daytime subcanopy respiration capturing microbial and root respiration—the dominant components of daytime R_e (Janssens et al., 2001; Law et al., 1999; Palmroth et al., 2005), and decomposition of coarse and fine woody debris and autotrophic respiration

from low understorey or groundcover vegetation. Although, the subcanopy observations would also include photosynthesis from this understorey (see Section 5.2), the respiration signal still primarily reflects the microbial decomposition and root respiration. The upper height limit of the subcanopy can be estimated by the height of the short understorey vegetation that is clearly separated from the tree canopy by substantial bole space, i.e., a few meters above ground. This proposed method combines conditional sampling approaches, quadrant analysis (Shaw et al., 1983; Wallace et al., 1972; Willmarth and Lu, 1974), and relaxed eddy accumulation (REA; Businger and Oncley, 1990) using CO_2, water vapour and vertical velocity time series from conventional high frequency EC measurements to derive independent estimates of daytime subcanopy respiration. The conceptual framework assumes that organized updrafts carry an unambiguous imprint of the different and representative sinks and sources of CO_2 and water vapour within the canopy volume. This proposed method is not intended to substitute for other existing approaches described earlier, but aims at providing additional constraints on daytime R_e estimates using EC data currently available at a large number of flux sites.

This new method was tested against datasets from four coniferous and one deciduous site in North America and Europe (four AmeriFlux sites, one Fluxnet site) most of them providing EC flux measurements at multiple levels. The success of the method will be determined by the general agreement among two criteria that have inherently different assumptions: daytime respiration estimates from the new method will be compared to: (i) the intercept of light-response curves (F_N versus shortwave down-welling radiation) to compare bulk respiration estimates over longer time scales (weeks to month) and (ii) CO_2 flux estimates measured by soil efflux chambers to directly compare respiration estimates on smaller time scales (half-hourly to daily). We will also explore potential skill predictors and limitations to this method.

2. Theory

The formal definition of the net turbulent CO_2 flux from EC technique is $F_{N,EC} = \overline{w'c'}$, where w is the turbulent vertical velocity ($m\,s^{-1}$) with $\overline{w} = 0$, c the turbulent CO_2 density ($\mu mol\,m^{-3}$), and primes and overbars are excursions from temporal mean and temporal averaging, respectively. This averaging does not lend itself to a formal decomposition into its component fluxes photosynthesis (F_A) and respiration (R_e). However, perturbations in concurrent water vapour density measurements q' ($mmol\,m^{-3}$) may provide an independent dataset that permits distinguishing between updraft events ($w' > 0$) simultaneously enriched in CO_2 ($c' > 0$) and water vapour ($q' > 0$) from other updraft and downdraft ($w' < 0$) events assuming the canonical mean density profiles of CO_2 and water vapour at daytime.

2.1. Conceptual framework

The conceptual framework of the new method, revised from Scanlon and Albertson (2001), links concentration perturbations to canonical mean concentration profiles (Fig. 1). Four quadrants (labeled Q1–Q4) are constructed in the c'–q' plane with events satisfying Q1: $c' > 0$ and $q' > 0$; Q2: $c' < 0$ and $q' > 0$; Q3: $c' < 0$ and $q' < 0$; and Q4: $c' > 0$ and $q' < 0$. During daytime conditions, when both photosynthesis and evapotranspiration are large, downdrafts ($w' < 0$) arrive at the measurement height enriched in CO_2 ($c' > 0$) but depleted in water vapour ($q' < 0$) compared to the within-canopy air, and therefore contribute to Q4. Updraft events ($w' > 0$) of air originating from the foliage are likely to be depleted in CO_2 ($c' < 0$) due to photosynthesis but enriched in water vapour ($q' > 0$) due to transpiration, thereby contributing to Q2. If the foliage is the only source and sink for water vapour and CO_2, respectively, we expect the correlation coefficient between c' and q' ($r_{c,q}$) to approach -1 during daytime. However, updraft events originating from the subcanopy are likely to be enriched in both CO_2 and water vapour ($c' > 0$ and $q' > 0$) as they carry the imprint of respiration and soil evaporation. These events therefore contribute to Q1 and cause a decorrelation between c' and q' leading to $r_{c,q} > -1$. Based on this conceptual framework, updrafts coming from the subcanopy and from the tree canopy can be identified and differentiated in the time series when they occur in Q1 and Q2. The necessary assumption is that air that has picked up qualities from the tree canopy on one hand, and the subcanopy on the other hand is not fully mixed, but are transported in separate, identifiable, confined eddies.

One must exercise caution when connecting the decorrelation in $r_{c,q}$ exclusively to the dissimilarity in scalar sinks/sources in the canopy sublayer, as other processes may have the same effect. Entrainment of air from the top of the atmospheric boundary layer may contribute to a decorrelation signal and was observed in flows close to the ground surface (Asanuma et al., 2007; DeBruin et al., 1991, 1999; Mahrt, 1991). However, decorrelation due to entrainment is likely to occur in downdrafts ($w' < 0$), whereas a decorrelation due to differences of the sinks/source distribution discussed here is expected to occur in updrafts ($w' > 0$). We here assume that entrainment processes play an insignificant role for scalar–scalar correlations in forests, which becomes important when using $r_{c,q}$ as universal indicator to predict the time fraction of respiration events in Q1 (see Section 4.3.1).

2.2. Two possible respiration models

One approach to estimating daytime respiration from the w', c' and q' time series is to compute the turbulent flux using the conditional average of the covariance

$$R_{e,EC} = \frac{1}{N}\sum_{i=1}^{N} I(t_i)w'(t_i)c'(t_i) \quad (1)$$

where

$$I(t_i) = \begin{cases} 1 & \text{if } q'(t_i) > 0,\ c'(t_i) > 0,\ w'(t_i) > 0 \\ 0 & \text{otherwise} \end{cases} \quad (2)$$

is the indicator function for updraft events in Q1 of the c'–q' plane, and t_i is the discrete time for $i = 1, \ldots, N$, with N being the total size of the time series (e.g., 9000, 18,000 and 36,000 for a time series of 1800 s duration sampled at 5, 10 and 20 Hz,

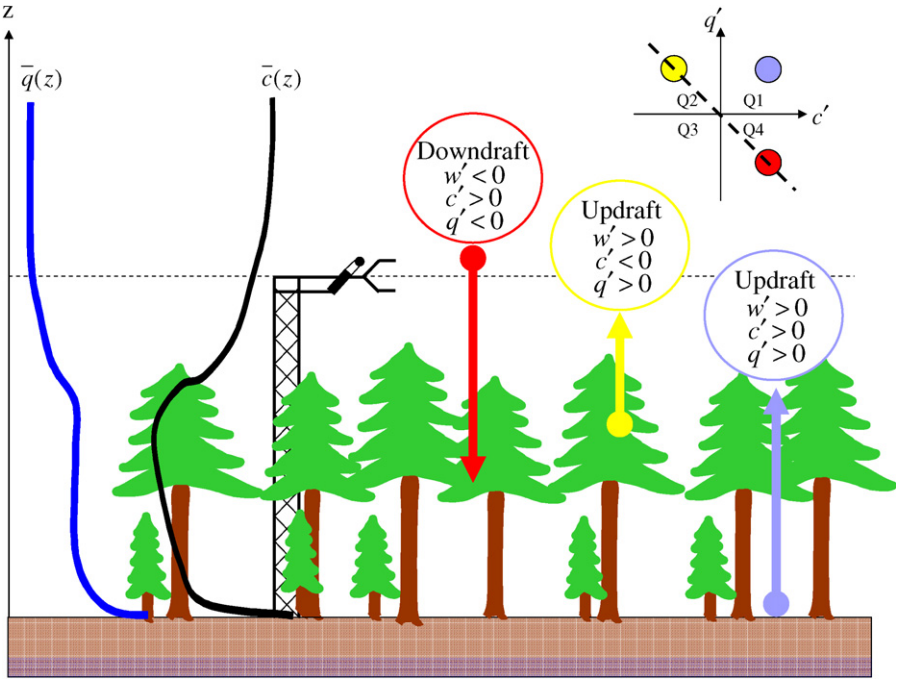

Fig. 1 – Conceptual model for the conditional sampling scheme. The surface layer similarity theory predictions (dashed line in the subplot) are shown in the idealized quadrant analysis when source (atmosphere) and sink (canopy) of carbon dioxide density c in quadrant Q4, and sink (atmosphere) and source (canopy) of water vapour density q in quadrant Q2 are identical. We propose to use updrafts occurring in quadrant Q1 to estimate daytime respiration R_e. The mean vertical profiles of c and q indicate idealized daytime conditions within the roughness sublayer assuming that the subcanopy is a source of both water vapour and CO_2.

respectively). As the indicator function $I(t_i)$ relies on the coherency between the water vapour and carbon dioxide exchange in updrafts coming from the subcanopy, it will primarily capture the respiration signal of microbial (litter, soil organic matter and woody detritus) and root respiration. Limitations of the method will be discussed in detail in Section 5.2. While this approach has some theoretical appeal, the time fraction of conditionally sampled R_e events is likely to be small during daytime conditions (i.e., <10%) thereby introducing small-size statistical convergence issues into the covariance (Eq. (1)). An alternative approach is to transform the computation of the covariance to a more robust measure such as the accumulation of concentrations, which will be explored now.

A second approach can be based on the traditional representation of the turbulent CO_2 flux utilising relaxed eddy accumulation (REA) technique (Businger and Oncley, 1990) given by

$$F_{N,REA} = \overline{w'c'} = \beta\sigma_w(\overline{c_+} - \overline{c_-}) = F_+ - F_-, \tag{3}$$

where σ_w is the standard deviation of the vertical velocity with $\sigma_w^2 = \overline{w'^2}$; $\overline{c_+}$ and $\overline{c_-}$ are the mean CO_2 densities in updrafts and downdrafts, respectively; F_+ and F_- are the total CO_2 fluxes in updrafts and downdrafts, respectively; and β is an empirical constant. If the relationship between c' and w' is close to linear, then β can be approximated by

$$\beta = \frac{\sigma_w}{\overline{w_+} - \overline{w_-}} \tag{4}$$

where $\overline{w_+}$ and $\overline{w_-}$ are the mean vertical velocities in updrafts and downdrafts, respectively. If the joint distribution of w' is Gaussian, then Eq. (4) predicts $\beta = 0.63$. Departures from a joint-Gaussian distribution generally lead to $\beta < 0.63$, often resulting in $\beta \approx 0.57$ (see, e.g., Table 1 in Katul et al., 1996; Ruppert et al., 2006).

For a stationary time series, the mean densities can be removed from $\overline{c_+}$ and $\overline{c_-}$, and these two terms can be expressed as c' in updrafts and downdrafts, respectively, by

$$\begin{aligned} F_{N,REA} &= \beta\sigma_w(\overline{c'_+} - \overline{c'_-}) \\ &= \beta\sigma_w \frac{\sum_{i=1}^{N} I_{w+}(t_i)c'(t_i)}{\sum_{i=1}^{N} I_{w+}(t_i)} - \beta\sigma_w \frac{\sum_{i=1}^{N} I_{w-}(t_i)c'(t_i)}{\sum_{i=1}^{N} I_{w-}(t_i)}, \end{aligned} \tag{5}$$

where

$$I_{w+}(t_i) = \begin{cases} 1 & \text{if } w'(t_i) > 0 \\ 0 & \text{otherwise} \end{cases} \tag{6}$$

and

$$I_{w-}(t_i) = \begin{cases} 1 & \text{if } w'(t_i) < 0 \\ 0 & \text{otherwise} \end{cases} \tag{7}$$

are the indicator functions for updrafts and downdrafts, respectively. Comparing the indicator functions for updrafts

only in Q1 $I(t_i)$ (Eq. (2)) and for updrafts in all quadrants (Q1–Q4) $I_{w+}(t_i)$ (Eq. (6)) yields that events sampled by $I(t_i)$ are a subset of those sampled by $I_{w+}(t_i)$ satisfying the additional constraints of $c' > 0$ and $q' > 0$. Thus, it is conceivable to formulate the respiration R_e as a component of the first right-hand side term of Eq. (5) given by

$$R_{e,REA} = \beta\sigma_w \frac{\sum_{i=1}^{N} I(t_i)c'(t_i)}{\sum_{i=1}^{N} I_{w+}(t_i)}. \quad (8)$$

The advantage of Eq. (8) over Eq. (1) is that it eliminates the need to compute a covariance from a limited sample size.

2.3. *Refined relaxed eddy accumulation model*

The conceptual framework (Section 2.1) can be tested by applying quadrant analysis to high-frequency time series of c' and q' to verify the existence of the hypothesized updraft respiration events in Q1 (Figs. 2 and 3). Most data populated quadrants Q2 and Q4 during daytime conditions as predicted by similarity theory, and the overall correlation coefficient of the distribution was $r_{c,q} < 0$. However, few excursions from similarity theory predictions occurred in Q1, which were exclusively associated with updrafts and led to a small decorrelation resulting in $r_{c,q} > -1$ (Fig. 2). No significant excursions were found in downdrafts (Fig. 3). The occurrence of this '*cloud*' shaped group of data validated the hypothesis that some updrafts carry the imprint of respiration processes from the subcanopy. This '*cloud*' group is the signal of interest and hence, need to be representatively sampled by the proposed respiration model. In some cases (Fig. 2b and d), a fraction of the '*cloud*' populated not only Q1, but also Q2 and will therefore not be included by our sampling scheme based on the indicator function $I(t_i)$ (Eq. (2)). The success of the model will depend on how representative the temporal mean $\bar{x}$ is when deriving the perturbations x' in each averaging period, i.e., the stationarity of the time series. Moreover, one needs to conclude that the two different types of updrafts defined in Fig. 1, one carrying the information of photosynthesis from the tree canopy and the other containing information of respiration from the subcanopy, merely represent the idealized end-members of a continuum of transient states in-between. We assume that some of the variation observed in Q1 could be attributed to changes in source strength with time or in sampling contrasting source areas in the flux footprint.

The probability density function of updrafts in the c'–q' plane (Fig. 2) also showed that a fraction of data in Q1 close the origin with approximately $p \geq 0.01$ obviously does not

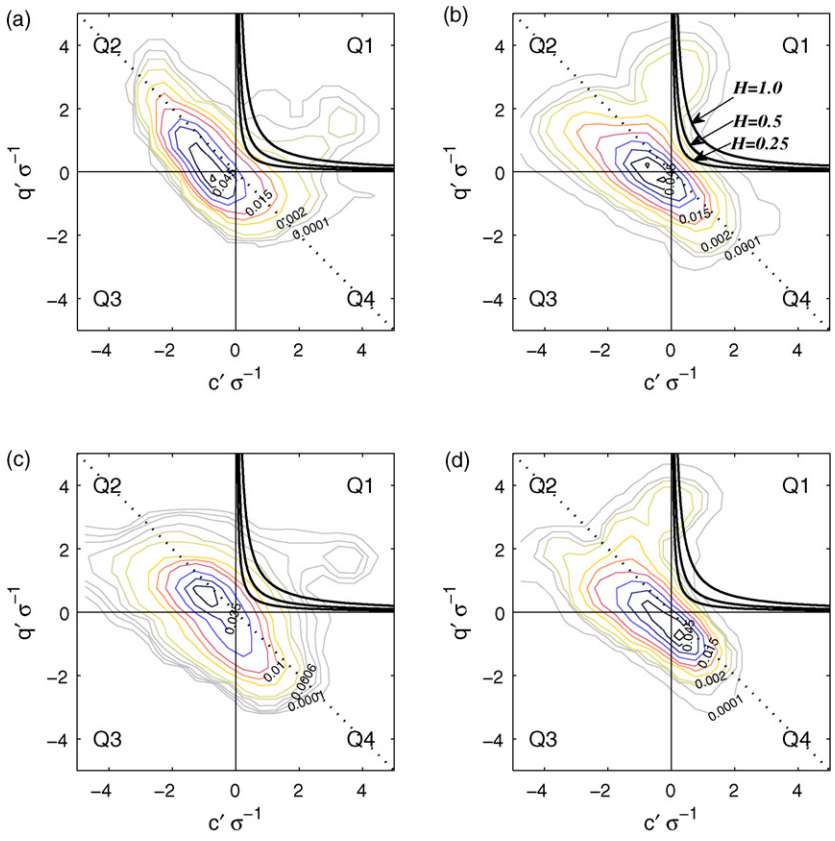

Fig. 2 – Contour plots of scalar–scalar probability density function of updrafts in normalized carbon dioxide c' and water vapour q' fluctuations recorded at sampling frequency listed in Table 2 for (a) DP04: May 10, 2004, 10:00–10:30 LST; (b) MFT: May 09, 2006, 13:00–13:30 LST; (c) MPT: June 23, 2006, 16:30–17:00 LST; (d) WS: July 07, 2003, 12:30–13:00 LST. Similarity theory predictions (dotted lines) are given for cases described in caption of Fig. 1. Also shown are hyperbolic deadbands *H* in quadrant Q1. See Section 2.3 for details.

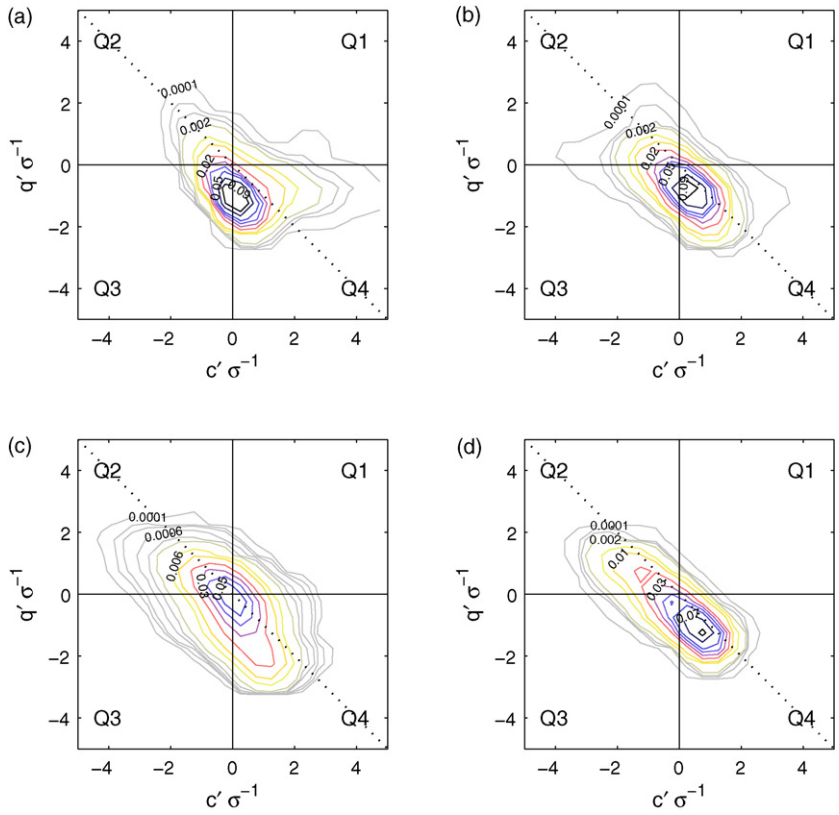

Fig. 3 – Contour plots of scalar–scalar probability density function of downdrafts for the same data used in Fig. 2.

belong to the '*cloud*' shaped excursions, but rather follows similarity theory predictions. However, those data would be sampled by $I(t_i)$ and hence, would affect the respiration estimates. We here introduce a hyperbolic threshold criterion H defined as

$$H = \frac{c'q'}{\sigma_c \sigma_q} \tag{9}$$

in Q1 to prevent contamination of respiration estimates by data obviously following similarity theory predictions and not departures from it. The sampling indicator functions (Eqs. (2) and (6)) need to be modified accordingly and are given by

$$I_H(t_i) = \begin{cases} 1 & \text{if } q'(t_i) > \dfrac{H}{c'(t_i)}, c'(t_i) > \dfrac{H}{q'(t_i)}, w'(t_i) > 0 \\ 0 & \text{otherwise} \end{cases} \tag{10a}$$

$$I_{H,w+}(t_i) = \begin{cases} 1 & \text{if } |c'(t_i)| > \left|\dfrac{H}{q'(t_i)}\right|, |q'(t_i)| > \left|\dfrac{H}{c'(t_i)}\right|, w'(t_i) > 0 \\ 0 & \text{otherwise} \end{cases} \tag{10b}$$

Thresholding data in a scalar–scalar (here c'–q') plane, and not in a velocity–scalar plane (e.g., w'–c') as commonly done in hyperbolic relaxed eddy accumulation (HREA, Bowling et al., 1999; Pattey et al., 1993; Ruppert et al., 2006), may introduce uncertainty into the REA formulation, as conditionally sampled, and therefore discontinuous scalar time series are combined with a continuous time series of the vertical velocity from which the empirical factor β (Eq. (4)) is calculated. Traditional HREA applies hyperbolic thresholds to the w'–c' plane in order to maximize the difference in mass accumulation for up- and downdrafts, and to relax the frequency at which the solenoids are required to open and close. Here, a new factor, β_H, is defined which is calculated only from w' data satisfying the hyperbolic threshold in the c'–q' plane. The comparison of the both factors expressed as the ratio $\beta_H \beta^{-1}$ yielded that the hyperbolic thresholds had little effect on the symmetry in the joint distribution of w' and resulted in deviations of $|(\beta - \beta_H)\beta^{-1}| \leq 5$ (%) for $H = 0.25$ (Fig. 4; Table 1). Deviations were observed to increase for increasing H. From this point onward, we will exclusively use the respiration model given by

$$R_{e,REA} = \beta_H \sigma_w \frac{\sum_{i=1}^{N} I_H(t_i) c'(t_i)}{\sum_{i=1}^{N} I_{H,w+}(t_i)} \tag{11}$$

with indicator functions given in Eqs. (10a) and (10b) to estimate daytime ecosystem respiration for all datasets. In most cases, respiration estimates will be presented for the smallest hyperbolic threshold tested, $H = 0.25$, as this value was found to efficiently exclude data following similarity theory predictions without significantly reducing the number of excursions sampled as the '*cloud*' shaped group. We will hereafter refer to the term '*respiration event*' as an episodic measurement event sampled by the refined REA model,

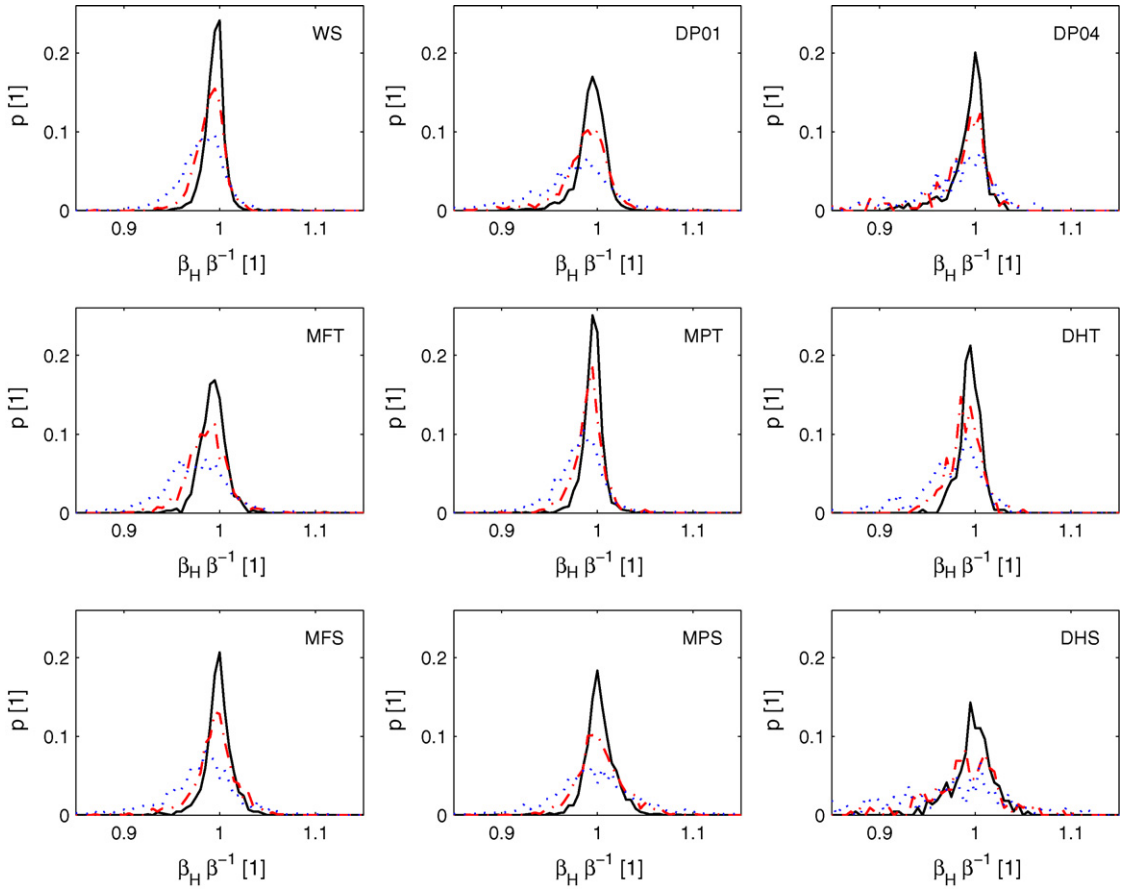

Fig. 4 – Probability density function of the ratio $\beta_H\beta^{-1}$ of selected datasets for hyperbolic threshold criteria $H = 0.25$ (solid black), $H = 0.5$ (dashed–dotted red) and $H = 1.0$ (dotted blue). The coefficient β in the REA formulation is given in Eq. (4), and β_H was calculated from vertical velocity data satisfying the hyperbolic threshold criterion in the c'–q' plane (see Section 2.3 for details).

acknowledging that the biological respiration process is continuous.

2.4. *Properties of respiration events*

When presenting and discussing the results, sampled respiration events will be characterized by two parameters: the time fraction of sampled respiration events τ_{R_e} in relation to the averaging length defined by

$$\tau_{R_e} = \frac{1}{N}\sum_{i=1}^{N} I_H(t_i) \tag{12}$$

and the time scale of respiration events D_{R_e}. The time scale of a single respiration event was calculated from

$$D_{R_e} = \frac{1}{f_s}\sum_{m=1}^{M} I_H(t_m) \tag{13}$$

where f_s is the sampling frequency of the time series, I_H the indicator function given in Eq. (10a) and M is the number of contiguous data sampled by I_H for the event. Consecutive individual events separated by less than $10\, f_s^{-1}$ were combined to allow for some stochastic noise and relax the number of very short events.

3. Datasets and data processing

The datasets selected to test this respiration model focused on forested canopy sites. Basic descriptions of the sites and datasets are listed in Table 2. Twelve datasets were selected

Table 1 – Median $\tilde{\mu}$ of the probability density function of factors β and β_H of the REA formulation for all datasets and different hyperbolic threshold criteria H

Site ID	$\tilde{\mu}_\beta$	$\tilde{\mu}_{\beta_H}$		
		$H = 0.25$	$H = 0.5$	$H = 1.0$
DHT	0.6376	0.6353	0.6319	0.6273
DHS	0.6518	0.6505	0.6470	0.6310
DP01	0.6407	0.6391	0.6373	0.6336
DP04	0.6407	0.6378	0.6346	0.6279
MFT	0.6316	0.6274	0.6236	0.6144
MFS	0.6501	0.6493	0.6464	0.6384
MPT	0.6363	0.6335	0.6312	0.6255
MPM	0.6555	0.6579	0.6574	0.6560
MPS	0.6518	0.6501	0.6486	0.6432
WS	0.6303	0.6273	0.6246	0.6207

See Section 2.3 for details and Table 2 for description of the datasets.

Table 2 – Sites and datasets selected to test the respiration model (Eq. (11))

ID	Site name/location	Period	Lat, Lon (°)	N_d	f_s (Hz)	z (m)	z_s (m)	h_c (m)	$p(\lvert h_c/L\rvert \le 0.5)$ (%)	$p(\lvert h_c/L\rvert \le 0.2)$ (%)	Major species	References
	Duke Hardwood	07.05.2006–13.05.2006	35.97N, 79.10W				0.1	33	74	46	*Quercus alba, Q. coccinea, Q. velutina, Carya tomentosa, C. ovata, Liriodendron tultipifera, Liquidambar styraciflua understorey: Cornus florida*	Stoy et al. (2006a)
DHT	Above canopy EC system			245	20	39.8						
DHS	Subcanopy EC system			208	20	7.3						
DP01	Duke Loblolly Pine, above canopy EC system	25.06.2001–10.08.2001	35.98N, 79.09W	1448	5	20.6	0.1	14	73	46	*Pinus taeda subcanopy: Acer rubrum, Ulmus alata, Cornus florida*	Stoy et al. (2006a,b)
DP04	Above canopy EC system	04.05.2004–13.05.2004		338	10	20.6			63	38		
	Marys River Douglas Fir	08.05.2006–04.06.2006	44.65N, 123.55W				0.02	26	77	50	*Pseudotsuga menziesii understorey: Gaultheria shallon*	None
MFT	Above canopy EC system			956	20	38.3						
MFS	Subcanopy EC system			862	20	4.0						
MFC	Soil CO_2 efflux chamber			1429		0.0						
	Metolius ponderosa pine	16.06.2006–16.07.2006	44.45N, 121.56W				0.02	20	76	52	*Pinus ponderosa, Calocedrus decurrens understorey: Purshia tridentata, Arctostaphylos patula*	Irvine et al. (2004)
MPT	Above canopy EC system			1320	20	33.5						
MPM	Midcanopy EC system			1256	20	10.0						
MPS	Subcanopy EC system			1168	20	4.0						
MPC	Soil CO_2 efflux chamber			1488		0.0						
WS	Waldstein Spruce, above canopy EC system	06.06.2003–31.07.2003	50.14N, 11.87E	1115	20	33.1	0.05	19	84	51	*Picea abies, understorey: Cala-magrostis vilosa, Deschampsia flexuosa, Vaccinium myrtillus*	Gerstberger et al. (2004)

Symbols are dataset identification label (ID), geographical latitude (Lat) and longitude (Lon), number of intervals with 1800 (s) averaging length (N_d), sampling frequency of turbulence measurements (f_s) and sampling height (z) above ground, depth of soil temperatures sensors (z_s), mean canopy height (h_c), percentage (p) of data in neutral ($\lvert h_c/L\rvert \le 0.2$) and near neutral ($\lvert h_c/L\rvert \le 0.5$) conditions. EC stands for eddy covariance.

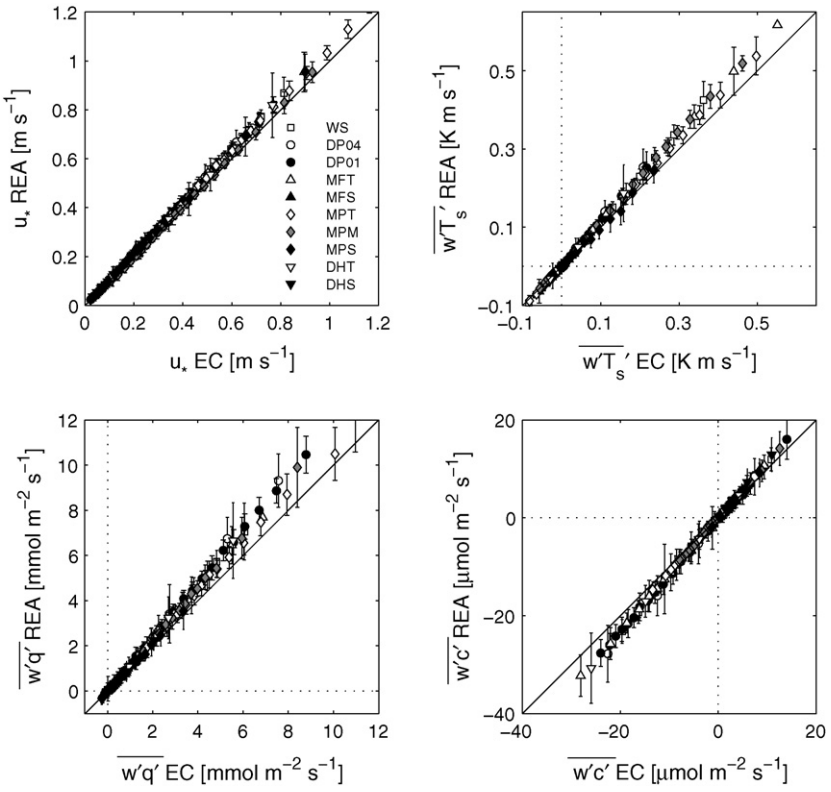

Fig. 5 – Comparison between relaxed eddy accumulation (REA) simulations and eddy covariance (EC) flux estimates of friction velocity (u_*), kinematic buoyancy flux $\overline{w'T'_s}$, kinematic latent heat flux $\overline{w'q'}$ and carbon dioxide flux $\overline{w'c'}$ for datasets listed in Table 2. To enhance the presentation of the large quantity of data, the original flux estimates over 1800 s were averaged into bins filled with an equal amount of data (n = 50) to avoid statistical uncertainties in error estimates among the bins. Vertical bars are ±1 standard deviation of the data in each bin; horizontal bars were not included to enhance clarity of presentation.

from five different sites with temperate climate, from which one had dominant deciduous species, and the remaining four were coniferous forests. Datasets from sites that typically experience a severe summer drought (e.g., MP site) were selected in such way that CO_2 and latent heat fluxes in the canopy and subcanopy/understorey were expected to be active, i.e., sufficient range in c' and q' during daytime conditions. The selected sites represent a wide range of canopy densities, from open and sparse canopies (e.g., MP, leaf area index, LAI, of 3.1 $m^2\ m^{-2}$), over moderate dense canopies (e.g., WS, LAI ≈ 5.2 $m^2\ m^{-2}$), to very dense canopies (MF, LAI ≈ 9.4 $m^2\ m^{-2}$). Differences in the vertical distribution of foliage were found between the deciduous and the coniferous forests, where coniferous trees had long clear boles with a vertical gap between understorey and overstorey leaf area. The differences in canopy morphology will be further described in the discussion of the results.

3.1. *Turbulence and radiation measurements*

Turbulent time series of CO_2 (c) and water vapour (q) densities were measured using an open-path infrared gas analyser (IRGA, model Li-7500, Lincoln, NE, USA) in combination with a three-dimensional sonic anemometer (model CSAT-3, Campbell Sci., Logan, UT, USA) for sampling the three-dimensional wind vector at all sites except for WS, where a different sonic anemometer was used (model Gill R3-30, Gill Instruments, Lymington, UK). Raw data from EC measurement systems were recorded at sampling frequencies between 5 and 20 Hz depending on the site. The wind vectors in each averaging period were rotated such that the mean cross-wind component and mean vertical wind equaled zero, i.e., $\overline{v} = 0$ and $\overline{w} = 0$, except for WS where a planar-fit rotation (Wilczak et al., 2001) was applied with rotation matrix $[b_0,b_1,b_2]$ determined over a 3-month period. Perturbations in turbulence observations were computed by applying Reynolds-decomposition, i.e., $x' = x - \overline{x}$, where the instantaneous reading x is decomposed into perturbation x' and temporal average $\overline{x}$, without the application of detrending algorithms. Time series of c and q collected from open-path IRGA were corrected for density fluctuations by multiplying the instantaneous scalar density reading by the ratio of mean to instantaneous density of moist air $\overline{\rho}_a/\rho_a$ calculated from the high-frequency time series of sonic temperature T_s and assuming isobaric conditions (see Detto and Katul, 2007 for details). This correction does not only alter the vertical covariances, but also higher order statistical moments such as variances and hence, the global correlation coefficient $r_{c,q}$. Turbulent flux estimates were then computed using: (i) covariances and (ii) the REA method (Eq. (3)) to obtain net

fluxes, and (iii) the respiration model given in Eq. (11) to arrive at component fluxes of daytime subcanopy respiration R_e. The length of the averaging period was consistently 1800 s. The coefficients β and β_H were computed for each averaging period from the raw data. As all flux calculation schemes assume stationary conditions and developed turbulence, fluxes were filtered for stationarity, integral turbulence characteristics, and plausibility limits (Foken et al., 2004).

Down-welling photosynthetic photon flux density (PPFD, μmol m^{-2} s^{-1}) above the canopy was either directly measured by sensors (DP, DH: model Li-190, Licor, Lincoln, NE, USA; MF, MP: model PARlite, Kipp & Zonen, Delft, Netherlands), or modeled from down-welling shortwave radiation measurements (WS: model CM 21, Kipp & Zonen, Delft, Netherlands). These data were used to estimate bulk ecosystem respiration from the intercept of the light-response curves.

3.2. Soil CO_2 efflux, temperature and moisture measurements

Soil temperatures at multiple depths were available at all sites measured by either thermocouples (MP, MF, DH and DP) or platinum resistance thermometers (WS). Soil temperatures were used from the depth closest to the ground surface at each site to find the functional relationship between soil CO_2 efflux and soil temperature assuming that it represents the zone of highest biological activity and contributes most to the respiration signal from the soil. Measurements of soil water content were made by time-domain reflectometry probes (model CS615, Campbell Sci., Logan, UT, USA) integrating over the upper 0.3 m of the soil at DP, MP and MF.

At MP and MF, soil CO_2 efflux is routinely measured using 6 automated chambers at the MF site and 10 at the MP site (each with 0.21 m^2 of soil surface area; Irvine and Law, 2002). Due to the length of the measurement cycle, site mean values of soil efflux were computed every 5400 and 7200 s at the MF and MP site, respectively; mean soil efflux estimates were synchronized to the turbulence data (1800 s) by linear interpolation. Monthly measurements of soil respiration from a spatially intensive array (25 measurement locations, manual instrument, model: Li-6400 with 6400-9 chamber, Licor, Lincoln, NE) were used to correct for biases in automated chamber location and technique.

4. Results

The validity of the traditional REA formulation was tested by comparing it to EC estimates for scalar fluxes and momentum exchange, separately for day- and nighttime conditions. The characteristics of the sampled respiration events were then discussed. Lastly, estimates of ecosystem daytime respiration were assessed through different independent indicators.

4.1. Testing the REA formulation by comparing $F_{N,EC}$ to $F_{N,REA}$

Before calculating daytime respiration fluxes from the here proposed refined REA approach, i.e., Eq. (11), it is imperative to test the robustness of the traditional REA. Generally, the EC method yielded consistently lower estimates of momentum and scalar vertical exchange of sensible and latent heat, and CO_2 compared to those from the REA for all datasets (Fig. 5). The higher REA estimates were caused by the simple model used to calculate β (Eq. (4)) that assumes a linear relationship between $\overline{w_+}$ and $\overline{w_-}$. Any curvature in the probability density function of the perturbations in vertical velocity will lead a value higher than its prediction of $\beta = 0.63$ for a truly symmetric Gaussian distribution. Fitting a linear regression to these data yielded that REA derived fluxes were higher than EC estimates by 2–10% for momentum transfer, and up to 21% for scalar fluxes (Table 3). Intercepts were negligible and all regressions significant. Largest departures from unity were site-specific (WS, DP04 and DHT) rather than height-dependent. The largest unexplained variability (lower coefficients of determination r^2) were observed from subcanopy EC systems of dense canopy sites (DHS and MFS), suggesting that the weak turbulence in the canopy volume may not adequately fulfill the assumptions of EC and REA.

4.2. Comparing nighttime respiration ($R_{e,EC}$ and $R_{e,REA}$)

For the assessment of the respiration model, it is crucial to investigate how CO_2 fluxes from these two methods (EC and REA) behave for nighttime conditions. More specifically, it is necessary to verify that the assumptions of scalar-variance similarity in the REA, and stationarity of the time series in both EC and REA hold true for weaker nighttime turbulence. The

Table 3 – Statistics of the linear regression model ($x_{REA} = a x_{EC} + b$) fitted to the empirical data shown in Fig. 5

Site ID	u_*			$\overline{w'T_s'}$			$\overline{w'q'}$			$\overline{w'c'}$		
	a	b (m s^{-1})	r^2	a	b (K m s^{-1})	r^2	a	b (mmol m^{-2} s^{-1})	r^2	a	b (μmol m^{-2} s^{-1})	r^2
DHT	1.06	−0.006	0.99	1.18	0.000	0.99	1.18	0.010	0.99	1.17	0.000	0.99
DHS	1.06	0.002	0.97	1.02	0.000	0.96	1.10	−0.018	0.97	1.18	0.000	0.83
DP01	1.06	−0.002	1.00	1.16	0.001	1.00	1.18	−0.001	0.99	1.14	−0.001	0.98
DP04	1.09	−0.008	1.00	1.21	0.003	1.00	1.24	−0.006	0.99	1.21	−0.001	0.99
MFT	1.07	−0.003	1.00	1.13	0.001	1.00	1.15	0.030	0.98	1.13	0.000	0.96
MFS	1.10	−0.002	0.98	1.02	0.000	0.95	1.02	−0.006	0.95	1.15	0.000	0.94
MPT	1.05	−0.001	1.00	1.09	0.001	1.00	1.10	0.012	0.99	1.10	0.000	0.99
MPM	1.02	−0.006	1.00	1.13	0.003	1.00	1.15	−0.056	0.99	1.08	0.000	0.97
MPS	1.06	−0.001	1.00	1.00	0.000	0.98	1.03	−0.003	0.96	1.10	0.000	0.91
WS	1.07	−0.004	1.00	1.16	0.001	1.00	1.17	−0.018	0.98	1.16	0.000	0.98

Coefficient of determination (r^2) is also stated.

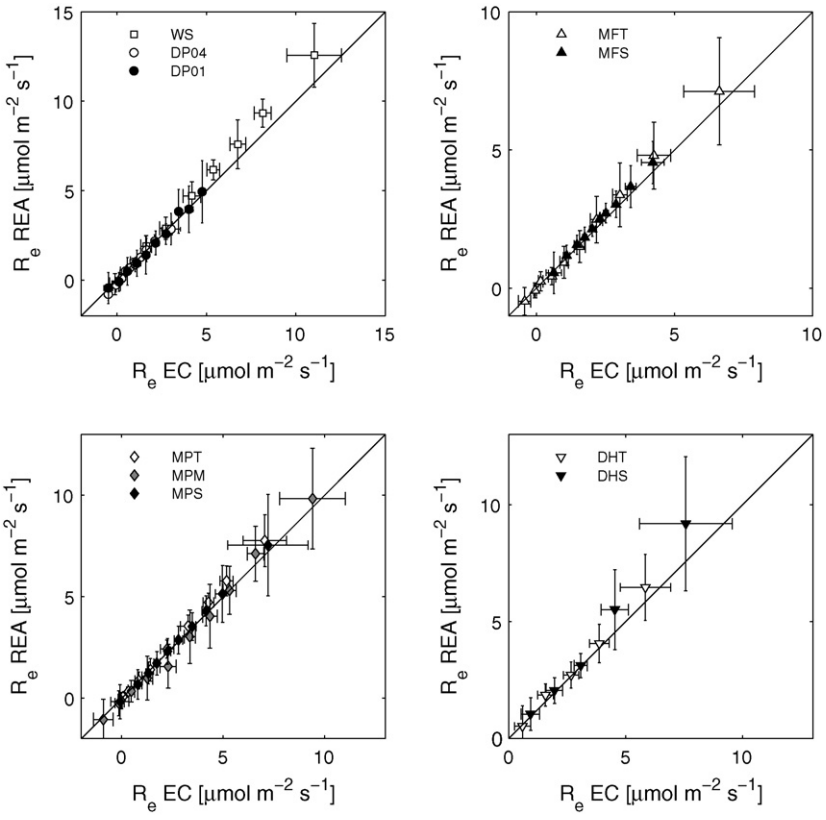

Fig. 6 – Flux estimates of ecosystem respiration R_e (=F_N), i.e., turbulent CO_2 flux at night (between 20:00 and 04:00 LST), using relaxed eddy accumulation (REA) and eddy covariance (EC) for datasets listed in Table 2. Individual estimates over an averaging period of 1800 s were grouped into bins with equal number of data (n = 10). Vertical and horizontal bars are ±1 standard deviation.

assumption of stationarity was verified by discarding data that did not pass the stationarity test (see Section 3.1), and the assumption of scalar-variance similarity in REA was indirectly tested by the comparison of its estimates to those of the EC method. Comparison of nighttime data showed that REA estimates tend to be larger than those from EC (Fig. 6), and thus confirmed the picture observed in the previous Fig. 5. Moreover, it emphasized the heteroscedastic nature of the scatter in nighttime CO_2 fluxes. No connection was found between the sampling height and the amplitude of observed nighttime R_e estimates at sites where measurements at multiple levels were available (MF, MP and DH). One would expect above canopy R_e estimates to be larger in magnitude than those calculated from the subcanopy, as the former accounts for both the subcanopy sources and respiration from stemwood and foliage. Contrary to this assumption, all potential combinations were found: (a) amplitude and magnitude of above-canopy R_e exceeded those for the subcanopy at MF, (b) amplitudes were similar for all heights at MP and (c) subcanopy R_e exceeded above-canopy R_e at DH.

4.3. *Statistics of sampled respiration events*

This section contains the statistical analysis of the characteristics τ_{R_e} and D_{R_e} (Section 2.4) for the daytime respiration events sampled by the model in Eq. (11).

4.3.1. *Connection between time fraction τ_{R_e} and global correlation coefficient $r_{c,q}$*

According to the conceptual framework, one would expect the '*cloud*' shaped group of respiration events in Q1 to effect decorrelation in daytime $r_{c,q}$. One would further assume that the decorrelation leads to more positive $r_{c,q}$ with growing time fraction τ_{R_e} (Eq. (12)). In agreement with these expectations, the computed relationship from the data between τ_{R_e} and $r_{c,q}$ was quasi-linear and appeared to be universal among all sites regardless of differences in ecosystem structure and function (Fig. 7). Maximum time fractions τ_{R_e} were 0.1 for daytime conditions with $r_{c,q} < 0$. At night ($r_{c,q} > 0$), the majority of the data is expected to populate Q1 and Q3 following similarity theory. The large observed time fractions $\tau_{R_e} \approx 0.15–0.2$ are therefore not surprising. It is worth noting that the scatter in τ_{R_e} appeared to be similar across the entire range except for $r_{c,q} < -0.75$, where the variability was diminished suggesting that respiration events in Q1 are inherently absent when the turbulent exchange approaches similarity predictions.

The global correlation coefficient $r_{c,q}$ therefore lends itself as a predictor to identifying periods when the time fraction of desired respiration events is large enough to extract a meaningful respiration signal, because it is universally connected to τ_{R_e}. In other words, no respiration signal can

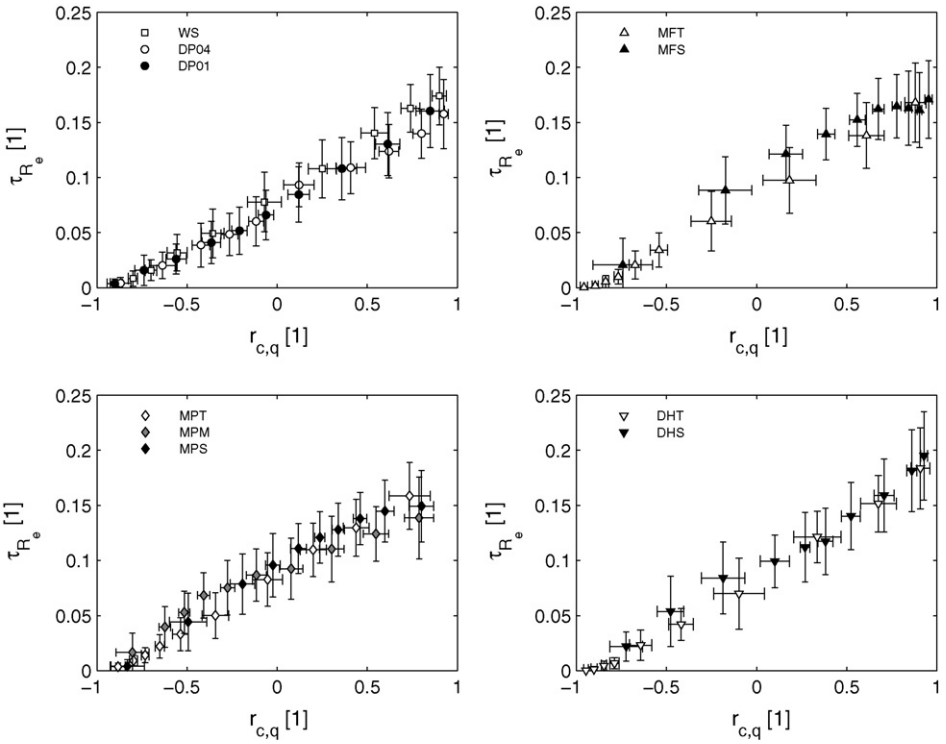

Fig. 7 – Time fraction τ_{R_e} (Eq. (12)) of respiration events in Q1 sampled by the refined REA model with $H = 0.25$ versus global correlation coefficient $r_{c,q}$. Individual data representing an averaging period of 1800 s were evenly distributed among a fixed number of bins ($n = 10$) and grouped. Bars are ±1 standard deviation.

be extracted from time series lacking a significant fraction of data in Q1 of the c'–q' plane. In the following, we chose a value of $r_{c,q} = -0.5$ as threshold based on Fig. 7 to filter datasets for periods likely to contain an extractable respiration signal from the subcanopy. Again, caution must be exercised when other processes such as entrainment, known to cause a decorrelation in $r_{c,q}$, are expected to modulate the turbulence in the canopy sublayer as stated earlier.

4.3.2. *Time scales of sampled respiration events*

The majority of sampled respiration events (≈60%) could be attributed to small-scale eddies with $D_{R_e} < 0.1$ s or <0.05 s depending on the sampling frequency (Fig. 8). Toward longer time scales, the probability density functions (pdf) of these events were nearly constant for $0.2 \leq D_{R_e} \leq 6$ s and then asymptotically approached zero for longer time scales. Little difference was observed between pdfs including day- and nighttime data (Fig. 8a), and daytime data only (Fig. 8b). Longer respiration events, i.e., larger D_{R_e} were more likely close to the respiration source as seen in the data from the subcanopy EC systems (MPS, MFS and DHS) compared to their levels above. This finding is readily explained as air from sources and sinks is progressively mixed when transported upward in the canopy volume leading to a dissection of formerly confined respiration pulses. It is worth noting that the contribution of individual respiration events to the total respiration flux from the subcanopy was inversely related to their probability of occurrence, i.e., few longer events contributed proportionally more to the total flux than abundant short events.

4.4. *Model assessment*

The proposed respiration model is assessed by means of two independent indicators to infer ecosystem respiration or its main components. These methods were selected because of their wide usage and application, and differences in their underlying assumptions and simplifications. As ecosystem respiration rates computed from any method can be reliably determined over longer time integrals only, we will focus on comparing time aggregates spanning several days to weeks.

4.4.1. *Comparison with intercept of light-response curves*

Light-response curves can be used to derive a bulk respiration flux R_0 by extrapolating the non-linear relationship between F_N and measured down-welling photosynthetic photon flux density (PPFD) during the day on to PPFD = 0, i.e., by determining the intercept with the y-axis. The method can be applied to either cloudless individual days to derive a bulk daily respiration, or to aggregated datasets over longer periods to derive a long-term average of R_0. The non-linear shape of the light-response curve was proposed by Ruimy et al. (1995), its intercept used for the correction of nighttime EC data by Lee et al. (1999), and was validated against higher order closure model calculations for DP (Juang et al., 2006). Here, this method is used to assess the performance of the proposed daytime respiration model. Specifically, the base respiration rate R_{10} determined from an exponential-type model (van't Hoff, 1898) defined as

$$R_e = R_{10} e^{\gamma(T-10/10)}, \quad (14)$$

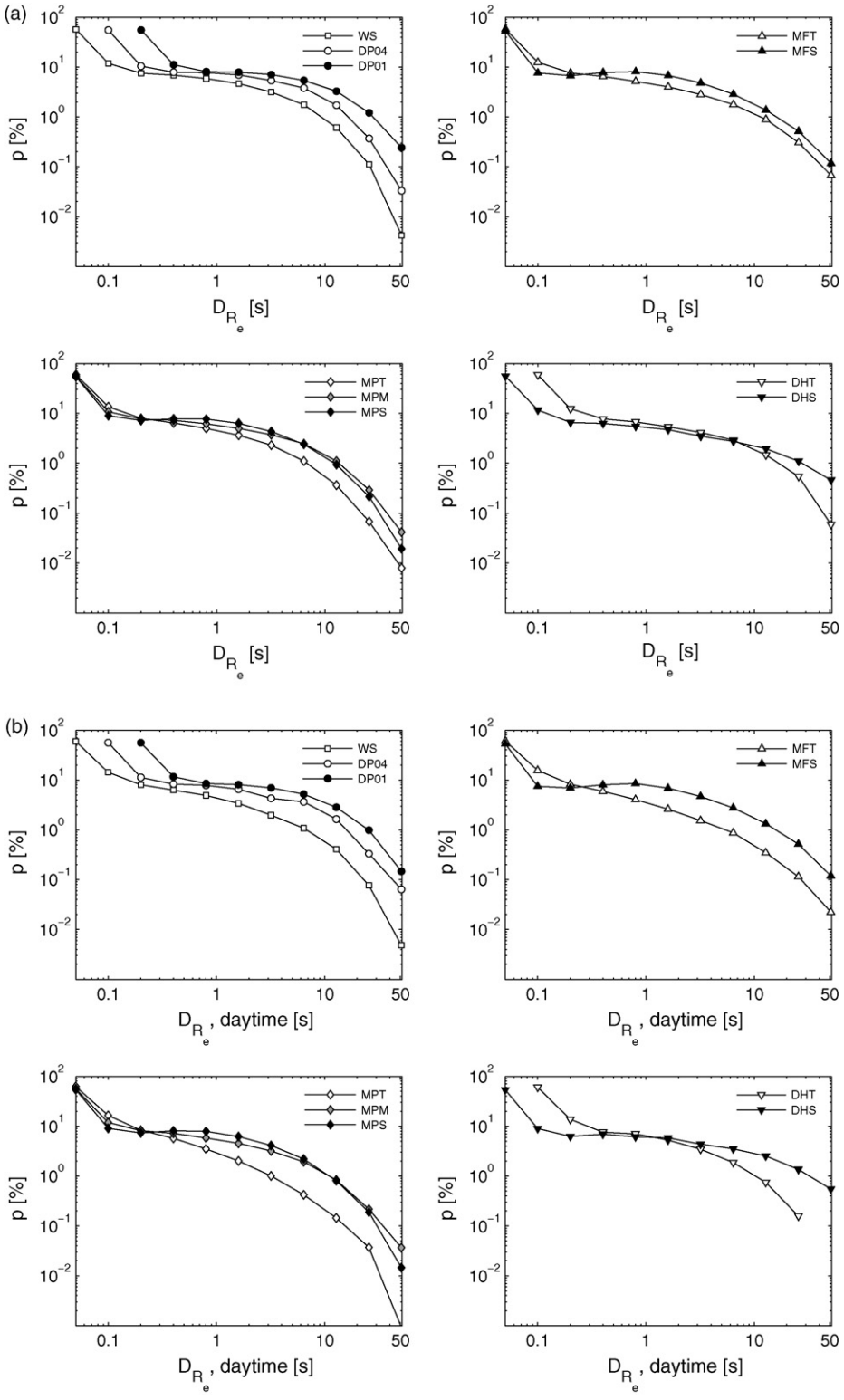

Fig. 8 – Probability density function of time scales D_{Re} (Eq. (13)) of respiration events sampled by the refined REA model with $H = 0.25$ for (a) day- and nighttime data combined, and (b) daytime data only. Individual data were grouped into bins of dyadic time scales.

with $e^{\gamma} = Q_{10}$, and temperature sensitivity Q_{10}, and air temperature T (°C) fitted to our daytime respiration estimates will be compared to the bulk respiration rates R_0 determined from the light-response curves (Fig. 9). Although, the two variables R_0 and R_{10} stem from different methods and are subject to different assumptions, they both represent estimates of bulk-respiration rates and thus may be used for a comparison of methods across sites.

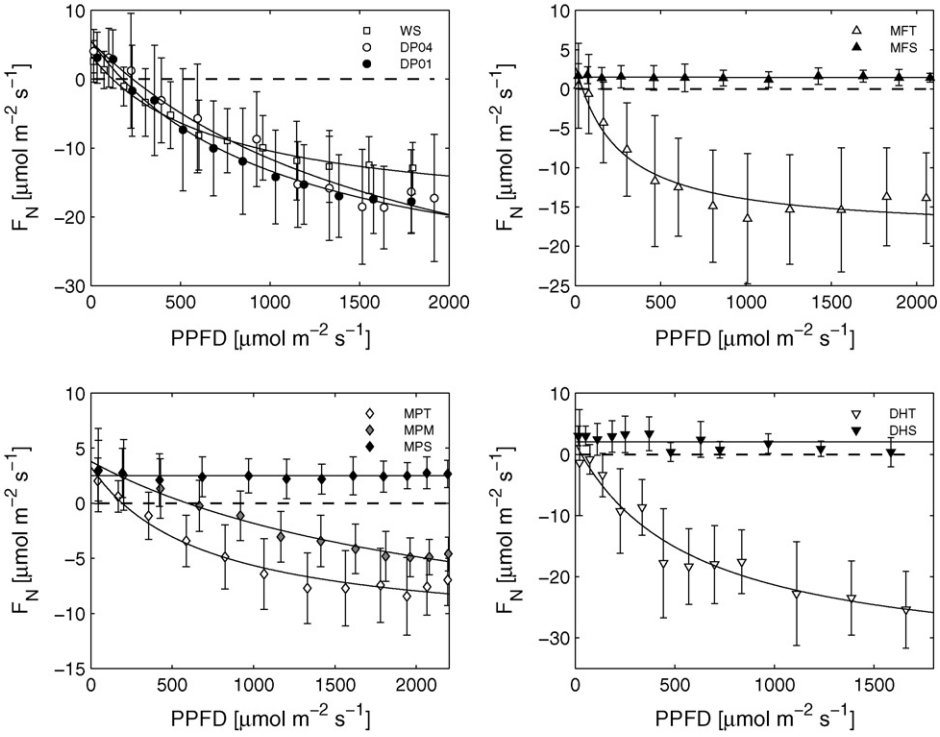

Fig. 9 – Net CO_2 flux (F_N) versus down-welling photosynthetic photon flux density (PPFD) recorded above the canopy for daylight conditions (PPFD > 5 µmol m^{-2} s^{-1}). Solid curves are fitted models of a Michaelis–Menthen type equation, see Table 4 details. Individual data representing an averaging period of 1800 s were evenly distributed among a fixed number of bins (n = 12) and grouped. Bars are ±1 standard deviation.

The comparison showed a good agreement between estimates computed from both methods (Table 4) when filtering with $r_{c,q} \geq -0.5$ as described in Section 4.3.1. Normalized differences Δ (see caption of Table 4 for definition) exceeding 60% were found only in case of three datasets (DHT, DP01 and WS). Generally, values of R_{10} were larger than R_0 resulting in $\Delta < 0$. However, even differences $\Delta \approx 100\%$ can be considered as realistic when taking into account that the listed R_{10} values represent a base respiration rate at a reference temperature of 10 °C, whereas R_0 is temperature independent, but depends on solar radiation only. Hence, the difference between both variables is expected to scale with the difference between the average temperature of each dataset and the chosen reference temperature.

4.4.2. *Comparison with soil CO_2 efflux chambers*

Soil CO_2 efflux is typically the largest contributor to ecosystem respiration compared to its other components (Janssens et al., 2001; Law et al., 1999; Palmroth et al., 2005). It is therefore conceivable that the success of the proposed respiration model considering subcanopy respiration can be further assessed by comparing its results to independent estimates from soil CO_2 efflux chambers where available (MFC and MPC).

The direct comparison of daytime respiration estimates calculated from the refined REA method and soil CO_2 efflux measurements showed a good agreement when the hyperbolic threshold criterion was chosen to be H = 0.25 (Fig. 10). The absence of any hyperbolic threshold (H = 0) resulted in underestimation, and larger hyperbolic thresholds $H \geq 0.5$ to overestimation compared to the chamber estimates. This observation confirmed our selection of H = 0.25 estimated from visual inspection of Fig. 2 as a robust threshold yielding realistic respiration estimates. It is worth noting that the variability in R_e calculated from the refined REA method expressed through the vertical bars was much larger compared to that in the soil CO_2 efflux rates. However, this observation is not surprising considering that the soil CO_2 efflux rates represent a spatial and temporal average computed from multiple individual chambers aggregated over longer periods than the averaging period chosen for the R_e estimates (1800 s). Hence, time series and response to changes in environmental drivers of soil CO_2 efflux appeared to be much smoother than for the daytime respiration estimates from the subcanopy.

5. Discussion

The results presented in the previous section suggested that the proposed model of the refined REA formulation with a hyperbolic threshold of H = 0.25 produced meaningful daytime respiration estimates at three out of five sites (DP, MF and MP). We will now focus on possible transporting mechanisms for the sampled respiration events, discuss the limitations of the model approach and explore indicators that could inform us about its likely success or failure in a given canopy prior to evaluation.

Table 4 – Coefficients of the Michaelis–Menthen type model $F_N = (\alpha PPFD/(\alpha PPFD + F_{csat})) + R_0$ fitted to the data displayed in Fig. 9, where α is photon-use efficiency, F_{csat} saturation net CO_2 flux, R_0 bulk respiration, PPFD photosynthetic photon flux density, and F_N net daytime CO_2 flux

Site ID	α	F_{csat} ($\mu mol\ m^{-2}\ s^{-1}$)	R_0 ($\mu mol\ m^{-2}\ s^{-1}$)	R_{10} ($\mu mol\ m^{-2}\ s^{-1}$)	Δ (%)
DHT	−0.063	−36.54	1.79	3.48	(−95)
DP01	−0.037	−38.60	5.60	14.45	(−158)
DP04	−0.027	−47.88	5.49	8.13	−48
MFT	−0.082	−20.73	2.56	3.99	−55
MPT	−0.022	−15.18	3.32	3.02	9
MPM	−0.008	−18.76	3.80	4.05	−7
WS	−0.034	−23.78	3.46	6.43	(−85)

Listed are also base respiration rates R_{10} derived from fitting Eq. (14) to the daytime R_e estimates calculated from the refined REA model (Eq. (11)) filtered for $r_{c,q} \geq -0.5$. The difference between the models was computed as $\Delta = (R_0 - R_{10})R_0^{-1} \times 100\%$, and values of $\Delta > 60\%$ are given in parentheses.

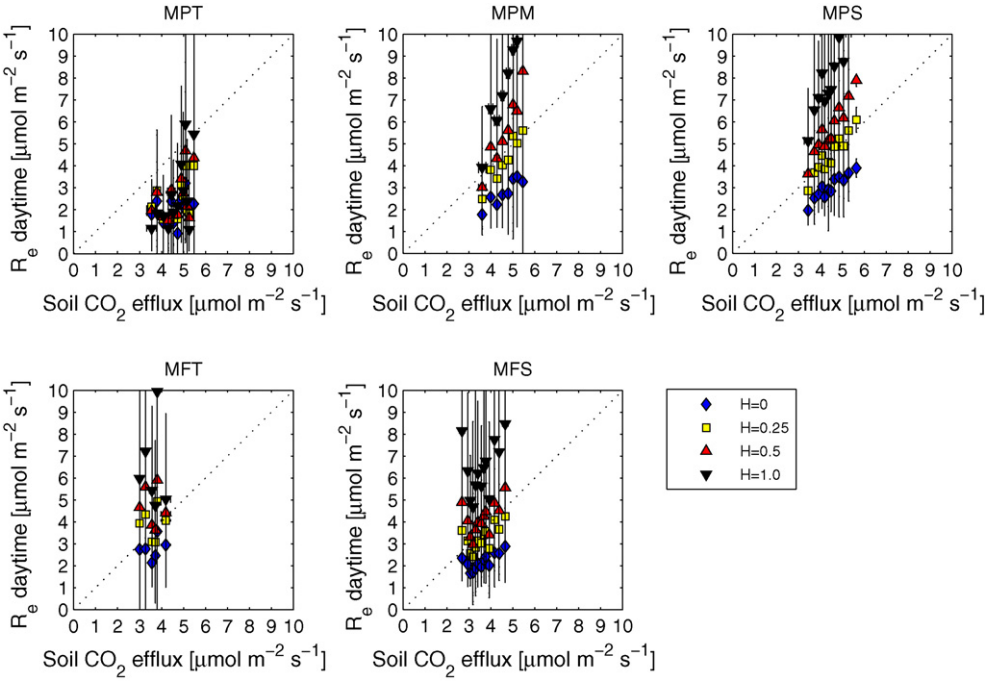

Fig. 10 – Daytime R_e estimates calculated from the refined REA model (Eq. (11)) filtered for $r_{c,q} \geq -0.5$ versus measurements of soil CO_2 efflux from chambers for varying hyperbolic threshold criteria H applied to the c'–q' plane. Individual data were grouped into bins each containing an equal amount of data ($n = 40$). Bars are ±1 standard deviation.

5.1. *Transport mechanism*

According to our conceptual framework, air containing CO_2 and water vapour from sources close to the forest floor and the subcanopy must be transported through the canopy and past our sensor before being substantially mixed with air carrying the signal of different sources and sinks present in the canopy volume. One therefore assumes that the eddies transporting the respiration and evapotranspiration signals may stay well structurally confined as they evolve in space and time—a definition used for coherent structures (Blackwelder and Kaplan, 1976). It is conceivable that respiration events sampled by the method proposed here are associated with the occurrence of coherent structures, specifically with the ejection phase when air is transported out of the canopy at moderate positive vertical velocities. Here, we define coherent structures as an aperiodic, but organized pattern in the turbulent flow with time scales of several 10 s consisting of a moderate upward motion (ejection, burst) ejecting air out of the canopy followed by a rapid downward motion (sweep, gust) injecting air into the canopy. Coherent structures often assume an asymmetric ramp-like shape in scalar time series, and a more symmetric triangle-like shape in those of wind vector components. If a single coherent structure was able to transport air from the subcanopy to the height just above the canopy, then a rough estimate of the time needed for the vertical transport can be derived as follows: the typical time scales of vertical velocities within coherent structures is

approximately 25 s (Thomas and Foken, 2007b), which is here assumed to be evenly divided into ejection and sweep phases. Scales of vertical transport assume velocities of several m s^{-1} throughout the canopy, whereas the tail-ends of probability density functions in the canopy tend to indicate more extreme events compared to its above-canopy equivalents. Assuming a mean vertical velocity of 2 m s^{-1} within coherent structures, a single structure could lift eddies up to 25 m. Given this unrefined assumption, one may think that coherent structures can be the underlying transporting mechanisms of the sampled respiration events. Referring to the results of the calculated time scales D_{R_e} (Fig. 8), a significant fraction of the distribution was occupied by events with $0.2 \leq D_{R_e} \leq 6$ s. Estimating the duration of the ejection phase as ≈13 s from such coarse calculation, the sampled respiration events supposedly connected to coherent structures would occupy up to half the length of the ejection phase, which seems realistic. The contribution of longer events to total subcanopy respiration was also disproportionately large compared to their frequency of occurrence. We further assume that the vertical lifting of air in the ejection phase of one coherent structure observed at the tower is caused by an injection of air into the canopy (sweep phase) of a different coherent structure away from the tower. This injection displaces the air in the subcanopy that had a sufficiently large residence time to accumulate the respiration signal of the subcanopy. The proposed transport mechanism of respiration events through coherent structures is in close agreement with a previous study of Scanlon and Albertson (2001) done at DP who also found that the data in Q1 of the c'–q' plane were primarily associated with data in Q4 ($w' > 0$ and $u' < 0$) of the w'–u' plane indicating an ejection motion. By relating the rate of turbulent kinetic energy (TKE) production to the time fraction of respiration events in Q1 of the c'–q' plane, the authors demonstrated that the turbulent motion of the air observed by their above canopy EC system was directly connected to the vertical transport of the respiration signal from the subcanopy. The eddy scales associated with the transport of air from the subcanopy were on the order of or smaller than the canopy height h_c in contrast to the dominant eddy size of approximately $4h_c$ responsible for the net exchange of CO_2 and water vapour between the atmosphere and the canopy.

5.2. *Limitations of the model*

Limitations to the proposed model arise from theoretical considerations of the conceptual framework. Because the coherence between CO_2 and water vapour transport in updrafts is crucial, any components of ecosystem respiration that do not leave a signal in both scalars will be systematically neglected. The respiration component of the woody tissue is less likely to be captured by our method, as it contributes to c', but not q'. The fraction of respiration from woody tissue to ecosystem respiration is typically small (compared to other autotrophic organs or heterotrophic respiration), and thus represents a minor source of error.

An actively photosynthesizing understorey can have a more severe effect: eddies enriched in CO_2 and water vapour coming from the subcanopy can be depleted in CO_2 as they traverse through the subcanopy resulting in $c' < 0$ or a decrease in magnitude of $c' > 0$, but are additionally enriched in water vapour through plant transpiration of the understorey leaving $q' > 0$. This refixation of respiratory CO_2 from the soil and other respiratory organs such as stems, branches and leaves by the understorey (CO_2 recycling) either leads to a failure of our sampling scheme, or may lead to a substantial underestimation. The fraction of recycled respiratory CO_2 was reported to range between 31% and 39% in closed tropical rain forests with inhibited turbulent mixing (Loescher et al., 2003; Sternberg et al., 1997), but to be negligible in an open tropical rain forest where turbulent mixing was maximized (Sternberg et al., 1997). Significantly lower values were calculated for different seasonal tropical forests (≈7–8%, Sternberg, 1989), a *Pinus resinosa* forest (≈9%, Flanagan and Varney, 1995) and cool-temperate deciduous forest (≈15%, Kondo et al., 2005). Given the transport mechanism discussed above, it seems logical that the magnitude of CO_2 refixation increases with a reduced depth of penetration of coherent structures into the canopy (Thomas and Foken, 2007a) leading to inhibited mixing and longer residence times of air close to the forest floor.

The sampling and/or canopy height may pose a constraint on the method proposed here. Above- and mid-canopy systems were found to have consistently smaller respiration estimates compared to their subcanopy equivalents possibly caused by: (i) increasing distance between the subcanopy and the sensor, which allows air from additional sinks and sources in the canopy to mix more substantially with the rising air; this progressive mixing with increasing distance from the subcanopy may weaken or ultimately lead to a removal of the '*cloud*' shaped group of data in Q1, and (ii) fewer intervals permitted by the filter $r_{c,q}$ lead to reduced statistical certainty of the bulk respiration estimate. The latter suggests that longer datasets are required to determine a meaningful functional relationship between ecosystem respiration and its environmental drivers, whereas the former might pose a direct limitation to the effectiveness of the method. Other limitations may arise from the canopy morphology and will be discussed below.

An investigation of scalar similarity in the turbulent exchange of CO_2, water vapour and sonic temperature for WS attributed observed dissimilarity primarily to the occurrence of coherent structures with event durations >60 s (corresponds to $f \leq 0.01$ Hz, where f is the natural frequency) (Ruppert et al., 2006). Moreover, spectral correlation indicated that scalar similarity may vary during the day with maximum agreement reached in the very early morning and afternoon hours between c and T_s, and around noon between c and q. One may speculate that the observed dissimilarity between c and q was caused to some degree by the respiration events in Q1, which were here demonstrated to cause a decorrelation in $r_{c,q}$. Hence, a high degree of spectral similarity between c and q may pose additional constraints on our method, as it may indicate periods when the time fraction of respiration events τ_{R_e} is too small to extract a meaningful daytime respiration signal.

5.3. *Skill indicators*

The likely connection between respiration events in updrafts sampled by the refined REA model and the occurrence of coherent structures makes it obvious that canopy morphology plays a significant role in success or failure of the model. On

one hand, the canopy must permit large eddies, such as coherent structures, to penetrate the canopy without being distorted and its turbulent kinetic energy (TKE) rapidly shunted to dissipation scales through the drag of the canopy elements. On the other hand, the most prominent mechanism for the generation of coherent structures is the flow instability at the inflection point of the mean horizontal velocity profile (Raupach et al., 1996), and these shear induced large-scale events are likely to share the fate of rapid dissipation by interaction with the canopy elements.

The very large dissipation rate in the canopy means that the eddy decorrelation or relaxation timescale is given by

$$\tau = \frac{(1/2)\overline{u_i' u_i'}}{\varepsilon + W_D} \tag{15}$$

where $W_D \approx C_d a \bar{u} \overline{u_i' u_i'}$ is the rate at which turbulence works against form drag and loses TKE to heat and wake kinetic energy, ε the dissipation rate of TKE, $\overline{u_i' u_i'}$ the covariance of velocity components with i = 1–3 being the longitudinal, cross-wind and vertical velocity, respectively, C_d the bulk drag coefficient, $\bar{u}$ the mean horizontal wind speed, and factor a is a dimensionless coefficient describing the vertical distribution of the leaf area (defined below in more detail). Assuming $\varepsilon/W_D \ll 1$, then the decorrelation time scale, which is a measure of loss of coherency in time, can be approximated by

$$\tau = \frac{(1/2)\overline{u_i' u_i'}}{W_D} \approx \frac{1}{2C_d a \bar{u}}. \tag{16}$$

In a first approximation, one may define the adjustment length scale $L_d = \tau \bar{u}$ as the characteristic eddy size in equilibrium with the work done against the canopy drag. Substituting Eq. (16) for τ becomes

$$L_d \approx \frac{1}{2C_d a} \tag{17}$$

We compare this length scale to the shear length scale L_s produced by the inflection-point instability given by

$$L_s = \frac{\bar{u}}{(\partial \bar{u}/\partial z)_{z=h_c}}, \tag{18}$$

where the denominator is the vertical gradient of the mean horizontal wind speed at canopy height h_c. For a near-exponential mean velocity profile attenuated at a rate of $\chi = u_*/\bar{u}$, the above equation can be rewritten as

$$L_s = \frac{h_c}{\chi} \tag{19}$$

Hence, the ratio of both length scales is given by

$$\frac{L_s}{L_d} \approx \frac{h_c}{\chi} 2C_d a \approx 2C_d a h_c \frac{\bar{u}}{u_*}, \tag{20}$$

with $a \approx \mathrm{LAI}/d_c$, LAI being the peak one-sided leaf area index, and d_c the centroid of the leaf area index defined from the ground surface. One may hypothesize that if $L_s/L_d \gg 1$, eddies produced by the inflectional instabilities in the mean flow near the canopy top (e.g., mixing-layer eddies) remain coherent regardless of the mechanical work against the canopy elements. Hence, L_s/L_d can serve as a prognostic measure to assess whether the method proposed in this study is likely to be successful in a given canopy structure.

The ratio L_s/L_d evaluated for above-canopy measurements was smallest for the deciduous site (DHT), followed by the coniferous sites in the order of WS, DP and MPT, and largest for MFT (Table 5). Our method is therefore most likely to fail at the deciduous sites, which was demonstrated by the results here. However, no explanation can be deduced from L_s/L_d for the lack of agreement at WS.

An alternate indicator can be deducted from the classification of exchange regimes in the vertical transport of coherent structures derived for WS (Thomas and Foken, 2007a). This classification differentiates between five different exchanges regimes with progressive vertical coupling between the air-layers atop the canopy, the crown space where most of the leaf area in concentrated, and the subcanopy including the area of clear tree boles and the understorey. The end-members are defined as 'air atop the canopy is decoupled from air within the crown and subcanopy' and 'fully coupled conditions'. One may expect that their regimes Cs (coupled subcanopy by sweeps) and C (fully coupled canopy) may indicate periods when a substantial amount of data is expected to occur in Q1 forming the '*cloud*' shaped group. Contrary to these expectations, the time fraction τ_{R_e} was found to decrease with increased vertical coupling indicated by the exchange regimes for WS (Fig. 11). This observation suggests that degree of vertical coupling is inherently associated with the degree of vertical mixing in this canopy, and therefore underlines the

Table 5 – Canopy properties and flow statistics for selected above-canopy eddy covariance flux system (for details see Table 2): sampling height (z), mean canopy height (h_c), peak one-sided leaf area index (LAI), centroid of the leaf area density profile defined from the ground surface (d_c), mean ratio of mean horizontal velocity ($\bar{u}$) to friction velocity (u_*), bulk drag coefficient (C_d), and ratio of shear length scale (L_s) to adjustment length scale (L_d) defined in Eq. (20)

ID	z a.g.l. (m)	h_c (m)	LAI ($m^2\ m^{-2}$)	$d_c h_c^{-1}$	$\bar{u}u_*^{-1}$	C_d	$L_s L_d^{-1}$
DHT	39.8	33	3	0.8	4.64	0.2	7
DP01	20.6	14	5	0.5	4.06	0.2	16
DP04	20.6	14	5	0.5	4.01	0.2	16
MFT	38.3	26	9.4	0.7	4.38	0.2	24
MPT	33.5	20	3.1	0.4	5.88	0.2	18
WS	33.1	19	5.2	0.7	5.39	0.2	16

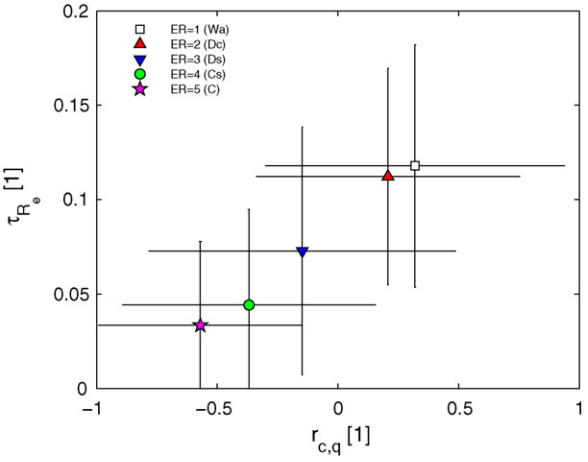

Fig. 11 – Time fraction τ_{R_e} (Eq. (12)) of respiration events in Q1 sampled by the refined REA model with H = 0.25 versus global correlation coefficient $r_{c,q}$ for WS grouped by different exchange regimes ER in the canopy (Thomas and Foken, 2007a). Vertical coupling in the canopy is negligible for ER = 1, 2 and progressively intensifies up to ER = 5 when the entire canopy is fully mixed. Error bars are ±1 standard deviation.

usefulness of the classification to diagnose vertical turbulent mixing. In other words, the more air-layers communicate, the more complete is the turbulent mixing which leads to a removal of excursions from similarity theory predictions on which the method proposed in this study relies. Moreover, periods characterized by a fully coupled canopy regime (C) were systematically precluded from analysis through filtering daytime R_e estimates for $r_{c,q} \geq -0.5$. This finding may explain the failure of the method at this particular site. Unfortunately, the classification of exchange regimes could not be applied to other datasets because of the lack of required measurements.

6. Conclusions

In conclusion, we expect the method to produce meaningful daytime estimates of subcanopy respiration in stands of low and moderate density with little understorey rather than in very dense, multi-layered canopies for the reasons discussed above. We further anticipate the method to be less successful in short canopies such as crops and grasslands, even though this has not been explicitly tested. Limitations in short canopies will be posed by the close proximity of sinks and sources of carbon dioxide and water vapour, and the intense turbulent mixing.

The usefulness of the method to directly compute a continuous time series of daytime respiration at high temporal resolution (i.e., half-hourly to hourly) is limited because only a subset of periods contain a respiration signal extractable by the employed conditional sampling scheme. Its strength lies in the direct determination of episodic estimates of daytime subcanopy respiration as the main component of ecosystem respiration from conventional EC measurements, which can then be combined to construct functional relationships between respiration processes and their meteorological and biological drivers.

Acknowledgements

This research was supported by the Office of Science (BER), U.S. Department of Energy (DOE, Grant nos. DE-FG02-06ER64318, DE-FG02-04ER63911 and DE-FG02-03ER63624), and the German Federal Department of Education and Research (Grant no. PT BEO51-0339476 D). Dr. G. Katul acknowledges support from the National Science Foundation (NSF-EAR 06-35787 and NSF-EAR-06-28432), the United States-Israel Binational Agricultural Research and Development (BARD, Research Grant No. IS3861-06), and the U.S. Department of Energy (DOE) through the office of Biological and Environmental Research (BER) Terrestrial Carbon Processes (TCP) program (Grant nos. 10509-0152, DE-FG02-00ER53015 and DE-FG02-95ER62083).

REFERENCES

Asanuma, J., Tamagawa, I., Ishikawa, H., Ma, Y.M., Hayashi, T., Qi, Y.Q., Wang, J.M., 2007. Spectral similarity between scalars at very low frequencies in the unstable atmospheric surface layer over the Tibetan plateau. Boundary Layer Meteorol. 122 (1), 85–103.

Blackwelder, R.F., Kaplan, R.E., 1976. On the wall structure of the turbulent boundary layer. J. Fluid. Mech. 76, 89–112.

Bowling, D.R., Delany, A.C., Turnipseed, A.A., Baldocchi, D.D., Monson, R.K., 1999. Modification of the relaxed eddy accumulation technique to maximize measured scalar mixing ratio differences in updrafts and downdrafts. J. Geophys. Res. Atmos. 104 (D8), 9121–9133.

Bowling, D.R., McDowell, N.G., Bond, B.J., Law, B.E., Ehleringer, J.R., 2002. C-13 content of ecosystem respiration is linked to precipitation and vapor pressure deficit. Oecologia 131 (1), 113–124.

Bowling, D.R., Tans, P.P., Monson, R.K., 2001. Partitioning net ecosystem carbon exchange with isotopic fluxes of CO_2. Global Change Biol. 7 (2), 127–145.

Businger, J.A., Oncley, S.P., 1990. Flux measurement with conditional sampling. J. Atmos. Ocean. Technol. 7, 349–352.

DeBruin, H.A.R., Bink, N.J., Kroon, L.J., 1991. Fluxes in the surface layer under advective conditions. In: Schmugge, T.J., André, J.C. (Eds.), Workshop on Land Surface Evaporation, Measurement and Parametrization. Springer, New York, pp. 157–169.

DeBruin, H.A.R., Van Der Hurk, J.J.M., Kroon, L.J.J.M., 1999. On the temperature–humidity correlation and similarity. Boundary Layer Meteorol. 93, 453–468.

Detto, M., Katul, G.G., 2007. Simplified expressions for adjusting higher-order turbulent statistics obtained from open path gas analyzers. Boundary Layer Meteorol. 122 (1), 205–216.

Ekblad, A., Hogberg, P., 2001. Natural abundance of C-13 in CO_2 respired from forest soils reveals speed of link between tree photosynthesis and root respiration. Oecologia 127 (3), 305–308.

Farquhar, G.D., Ehleringer, J.R., Hubick, K.T., 1989. Carbon isotope discrimination and photosynthesis. Ann. Rev. Plant Physiol. Plant Mol. Biol. 40, 502–537.

Flanagan, L.B., Varney, G.T., 1995. Influence of vegetation and soil CO_2 exchange on the concentration and stable oxygen

isotope ratio of atmospheric CO_2 within a *Pinus resinosa* canopy. Oecologia 101 (1), 37–44.
Foken, T., Göckede, M., Mauder, M., Mahrt, L., Amiro, B.D., Munger, J.W., 2004. Post-field data quality control. In: Lee, X., Massman, W.J., Law, B. (Eds.), Handbook of Micrometeorology: A Guide for Surface Flux Measurements. Kluwer, Dordrecht, pp. 181–208.
Gerstberger, P., Foken, T., Kalbitz, K., 2004. The Lehstenbach and Steinkreuz catchments in NE Bavaria, Germany. In: Matzner, E. (Ed.), Biogeochemistry of Forested Catchments in a Changing Environment. Ecological Studies, No. 172. Springer, Heidelberg, pp. 15–41.
Irvine, J., Law, B.E., 2002. Contrasting soil respiration in young and old-growth ponderosa pine forests. Global Change Biol. 8 (12), 1183–1194.
Irvine, J., Law, B.E., Kurpius, M.R., Anthoni, P.M., Moore, D., Schwarz, P.A., 2004. Age-related changes in ecosystem structure and function and effects on water and carbon exchange in ponderosa pine. Tree Physiol. 24 (7), 753–763.
Janssens, I.A., Lankreijer, H., Matteucci, G., Kowalski, A.S., Buchmann, N., Epron, D., Pilegaard, K., Kutsch, W., Longdoz, B., Grunwald, T., Montagnani, L., Dore, S., Rebmann, C., Moors, E.J., Grelle, A., Rannik, U., Morgenstern, K., Oltchev, S., Clement, R., Gudmundsson, J., Minerbi, S., Berbigier, P., Ibrom, A., Moncrieff, J., Aubinet, M., Bernhofer, C., Jensen, N.O., Vesala, T., Granier, A., Schulze, E.D., Lindroth, A., Dolman, A.J., Jarvis, P.G., Ceulemans, R., Valentini, R., 2001. Productivity overshadows temperature in determining soil and ecosystem respiration across European forests. Global Change Biol. 7 (3), 269–278.
Juang, J.Y., Katul, G.G., Siqueira, M.B.S., Stoy, P.C., Palmroth, S., McCarthy, H.R., Kim, H.S., Oren, R., 2006. Modeling nighttime ecosystem respiration from measured CO_2 concentration and air temperature profiles using inverse methods. J. Geophys. Res. Atmos. 111, D08S05.
Katul, G.G., Finkelstein, P.L., Clarke, J.F., Ellestad, T.G., 1996. An investigation of the conditional sampling method used to estimate fluxes of active, reactive, and passive scalars. J. Appl. Meteorol. 35 (10), 1835–1845.
Knohl, A., Buchmann, N., 2005. Partitioning the net CO_2 flux of a deciduous forest into respiration and assimilation using stable carbon isotopes. Global Biogeochem. Cycles 19 (4), GB4008.
Kondo, M., Muraoka, H., Uchida, M., Yazaki, Y., Koizumi, H., 2005. Refixation of respired CO_2 by understory vegetation in a cool-temperate deciduous forest in Japan. Agric. Forest Meteorol. 134 (1–4), 110–121.
Law, B.E., Kelliher, F.M., Baldocchi, D.D., Anthoni, P.M., Irvine, J., Moore, D., Van Tuyl, S., 2001. Spatial and temporal variation in respiration in a young ponderosa pine forests during a summer drought. Agric. Forest Meteorol. 110 (1), 27–43.
Law, B.E., Ryan, M.G., Anthoni, P.M., 1999. Seasonal and annual respiration of a ponderosa pine ecosystem. Global Change Biol. 5 (2), 169–182.
Lee, X.H., Fuentes, J.D., Staebler, R.M., Neumann, H.H., 1999. Long-term observation of the atmospheric exchange of CO_2 with a temperate deciduous forest in southern Ontario, Canada. J. Geophys. Res. Atmos. 104 (D13), 15975–15984.
Lin, G.H., Ehleringer, J.R., 1997. Carbon isotopic fractionation does not occur during dark respiration in C-3 and C-4. Plant Physiol. 114 (1), 391–394.
Lloyd, J., Taylor, J.A., 1994. On the temperature dependence of soil respiration. Funct. Ecol. 8, 315–323.
Loescher, H.W., Oberbauer, S.F., Gholz, H.L., Clark, D.B., 2003. Environmental controls on net ecosystem-level carbon exchange and productivity in a Central American tropical wet forest. Global Change Biol. 9 (3), 396–412.
Mahrt, L., 1991. Boundary-layer moisture regimes. Quart. J. R. Meteorol. Soc. 117, 151–176.
Ogee, J., Peylin, P., Ciais, P., Bariac, T., Brunet, Y., Berbigier, P., Roche, C., Richard, P., Bardoux, G., Bonnefond, J.M., 2003. Partitioning net ecosystem carbon exchange into net assimilation and respiration using (CO_2)-C-13 measurements: a cost-effective sampling strategy. Global Biogeochem. Cycles 17 (2), 1070 doi:10.1029/2002GB001995.
Palmroth, S., Maier, C.A., McCarthy, H.R., Oishi, A.C., Kim, H.S., Johnsen, K.H., Katul, G.G., Oren, R., 2005. Contrasting responses to drought of forest floor CO_2 efflux in a Loblolly pine plantation and a nearby Oak-Hickory forest. Global Change Biol. 11 (3), 421–434.
Pattey, E., Desjardins, R.L., Rochette, P., 1993. Accuracy of the relaxed eddy-accumulation technique, evaluated using CO_2 flux measurements. Boundary Layer Meteorol. 66 (4), 341–355.
Raupach, M.R., Finnigan, J.J., Brunet, Y., 1996. Coherent eddies and turbulence in vegetation canopies: the mixing-layer analogy. Boundary Layer Meteorol. 78, 351–382.
Rayment, M.B., Jarvis, P.G., 2000. Temporal and spatial variation of soil CO_2 efflux in a Canadian boreal forest. Soil Biol. Biochem. 32 (1), 35–45.
Reichstein, M., Falge, E., Baldocchi, D., Papale, D., Aubinet, M., Berbigier, P., Bernhofer, C., Buchmann, N., Gilmanov, T., Granier, A., Grunwald, T., Havrankova, K., Ilvesniemi, H., Janous, D., Knohl, A., Laurila, T., Lohila, A., Loustau, D., Matteucci, G., Meyers, T., Miglietta, F., Ourcival, J.M., Pumpanen, J., Rambal, S., Rotenberg, E., Sanz, M., Tenhunen, J., Seufert, G., Vaccari, F., Vesala, T., Yakir, D., Valentini, R., 2005. On the separation of net ecosystem exchange into assimilation and ecosystem respiration: review and improved algorithm. Global Change Biol. 11 (9), 1424–1439.
Ruimy, A., Jarvis, P.G., Baldocchi, D.D., Saugier, B., 1995. CO_2 fluxes over plant canopies and solar radiation: a review. Adv. Ecol. Res. 26, 1–68.
Ruppert, J., Thomas, C., Foken, T., 2006. Scalar similarity for relaxed eddy accumulation methods. Boundary Layer Meteorol. 120, 39–63.
Ryan, M.G., 1991. A simple method for estimating gross carbon budgets for vegetation in forest ecosystems. Tree Physiol. 9, 255–266.
Scanlon, T.M., Albertson, J.D., 2001. Turbulent transport of carbon dioxide and water vapor within a vegetation canopy during unstable conditions: identification of episodes using wavelet analysis. J. Geophys. Res. Atmos. 106 (D7), 7251–7262.
Sharp, R., Matthews, M., Boyer, J., 1984. Kok effect and the quantum yield of photosynthesis: light partially inhibits dark respiration. Plant Physiol. 75, 95–101.
Shaw, R.H., Tavangar, J., Ward, D.P., 1983. Structure of the Reynolds stress in a canopy layer. J. Clim. Appl. Meteorol. 22, 1922–1931.
Sternberg, L.D.L., 1989. A model to estimate carbon dioxide recycling in forests using 13C/12C ratios and concentrations of ambient carbon dioxide. Agric. Forest Meteorol. 48 (1/2), 163–173.
Sternberg, L.D.S., Moreira, M.Z., Martinelli, L.A., Victoria, R.L., Barbosa, E.M., Bonates, L.C.M., Nepstad, D.C., 1997. Carbon dioxide recycling in two Amazonian tropical forests. Agric. Forest Meteorol. 88 (1–4), 259–268.
Stoy, P.C., Katul, G.G., Siqueira, M.B.S., Juang, J.Y., Novick, K.A., McCarthy, H.R., Oishi, A.C., Uebelherr, J.M., Kim, H.S., Oren, R., 2006a. Separating the effects of climate and vegetation on evapotranspiration along a successional chronosequence in the southeastern US. Global Change Biol. 12 (11), 2115–2135.
Stoy, P.C., Katul, G.G., Siqueira, M.B.S., Juang, J.Y., Novick, K.A., Uebelherr, J.M., Oren, R., 2006b. An evaluation of models for partitioning eddy covariance-measured net ecosystem

exchange into photosynthesis and respiration. Agric. Forest Meteorol. 141 (1), 2–18.
Stoy, P.C., Palmroth, S., Oishi, A.C., Siqueira, M.B.S., Juang, J.Y., Novick, K.A., Ward, E.J., Katul, G.G., Oren, R., 2007. Are ecosystem carbon inputs and outputs coupled at short time scales? A case study from adjacent pine and hardwood forests using impulse-response analysis. Plant Cell Environ. 30 (6), 700–710.
Thomas, C., Foken, T., 2007a. Flux contribution of coherent structures and its implications for the exchange of energy and matter in a tall spruce canopy. Boundary Layer Meteorol. 123, 317–337.
Thomas, C., Foken, T., 2007b. Organised motion in a tall spruce canopy: temporal scales, structure spacing and terrain effects. Boundary Layer Meteorol. 122, 123–147.
van't Hoff, J.H., 1898. In: Lehfeldt, t.b.R.A.. (Ed.), Lectures on Theoretical and Physical Chemistry. Part I: Chemical Dynamics. Edward Arnold, London, pp. 224–229.
Wallace, J.M., Eckelmann, H., Brodkey, R.S., 1972. The wall region in turbulent shear flow. J. Fluid Mech. 54, 39–48.
Wichura, B., Ruppert, J., Delany, A.C., Buchmann, N., Foken, T., 2004. Structure of carbon dioxide exchange processes above a spruce forest. In: Matzner, E. (Ed.), Biogeochemistry of Forested Catchments in a Changing Environment. Ecological Studies, No. 172. Springer, Heidelberg, Berlin, pp. 161–176.
Wilczak, J.M., Oncley, S.P., Stage, S.A., 2001. Sonic anemometer tilt correction algorithms. Boundary Layer Meteorol. 99, 127–150.
Willmarth, W.W., Lu, S.S., 1974. Structure of the Reynolds stress and the occurrence of bursts in the turbulent boundary layer. In: Frenkiel, F.N., Munn, R.E. (Eds.), Turbulent Diffusion in Environmental Pollution. Academic Press, pp. 287–314.
Yakir, D., Sternberg, L.D.L., 2000. The use of stable isotopes to study ecosystem gas exchange. Oecologia 123 (3), 297–311.
Yakir, D., Wang, X.F., 1996. Fluxes of CO_2 and water between terrestrial vegetation and the atmosphere estimated from isotope measurements. Nature 380 (6574), 515–517.